Second International Symposium on Marine Propulsors
smp'11, Hamburg, Germany, June 2011

Numerical and Experimental Study on Ventilation for Azimuth Thrusters and Cycloidal Propellers

Michael Palm, Dirk Jürgens, David Bendl

Voith Turbo Schneider Propulsion GmbH & Co. KG, Heidenheim, Germany

ABSTRACT

On ships in rough water, the propellers can be subject to ventilation if the propulsors approach or break the water surface. The entrapped air results in large force and torque fluctuations which may lead to the power transmission system failing. Additionally, a ship with ventilating propellers will encounter thrust losses that will limit the maneuverability in rough seas.

Whereas many investigations into the ventilation behavior of azimuth thrusters were carried out in the past, no publications are known to the authors where cycloidal propellers, such as the Voith Schneider Propeller, have been examined in that regard.

With the help of scale model testing, the study on hand compares the ventilation characteristics of a rudder propeller to those of a Voith Schneider Propeller. The tests are supported by CFD calculations that reveal details of the flow mechanisms involved in propeller ventilation.

Keywords
Voith Schneider Propeller, Ventilation, Thruster

1 INTRODUCTION

Azimuth-steerable thrusters and cycloidal propellers are widely used for ship propulsion in many branches of the offshore industry. In many cases, these propellers are highly loaded. In combination with their vicinity to the free water surface, the propellers may be susceptible to ventilation. In this case, air is drawn into the propeller domain (Fig. 1) and has a significant impact on the hydrodynamic performance and mechanical loading.

Over the last decade in particular, many studies on the ventilation phenomenon have been conducted for azimuth thrusters.

It was shown that the dynamic fluctuations resulting from ventilation can vary from 0% to 100% of the force level of non-ventilating propellers (Koushan 2004). Detailed insight into the ventilation inception mechanism is given by time-lapse photographs for open and ducted thrusters by Koushan (2006a) and Koushan (2006b). Dynamic triggering of ventilation was achieved in Koushan (2006c) and Koushan (2007) by applying a forced sinusoidal heave motion on the thrusters, thus providing further insight into inception mechanisms.

A numerical approach to the ventilation phenomena was followed by Califano et al (2009). Here, a RANSE code was used to simulate ventilation effects on an open screw propeller.

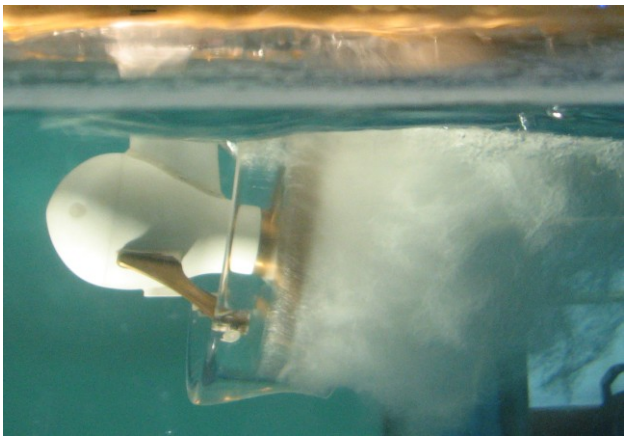

Fig. 1: Ventilating Azimuth Thruster

To gain some knowledge of the ventilation mechanisms for cycloidal propellers, the paper on hand shows some aspects of ventilation for this type of propulsor. For comparison reasons, the same tests were also conducted for an azimuth thruster.

The next section briefly introduces the solution method used. The subsequent sections describe the propellers used and present the results of the experimental and numerical studies. The final section summarizes the findings.

2 COMPUTATIONAL METHOD

All computations described here have been performed using the CFD software Comet. It is based on a finite-volume (FV) method and starts from conservation equations in integral form. With appropriate initial and boundary conditions and by using a number of discrete

approximations, an algebraic equation system solvable on a computer is obtained. First, the spatial solution domain is subdivided into a finite number of contiguous control volumes (CVs) which can be of an arbitrary polyhedral shape and are typically made smaller in regions of rapid variation of flow variables. The time interval of interest is also subdivided into time steps of appropriate size (not necessarily constant). The governing equations contain surface and volume integrals, as well as time and space derivatives. These are then approximated for each CV and time level using suitable approximations.

The flow is assumed to be governed by the Reynolds-averaged Navier-Stokes equations, in which turbulence effects are included via an eddy-viscosity model (k-ε or k-ω models are typically used). Thus, the continuity equation, three momentum component equations, and two equations for turbulence properties are solved. In addition, the space-conservation law must be satisfied as the CVs have to move and change their shape and location as the propeller starts to rotate. These equations are:

Mass conservation:

$$\frac{\mathrm{d}}{\mathrm{d}t}\int_V \rho \,\mathrm{d}V + \int_S \rho(\mathbf{v}-\mathbf{v}_\mathrm{b})\cdot\mathbf{n}\,\mathrm{d}S = 0$$

Momentum conservation:

$$\frac{\mathrm{d}}{\mathrm{d}t}\int_V \rho\mathbf{v} \,\mathrm{d}V + \int_S \rho\mathbf{v}(\mathbf{v}-\mathbf{v}_\mathrm{b})\cdot\mathbf{n}\,\mathrm{d}S = \int_S (\mathbf{T}-p\mathbf{I})\cdot\mathbf{n}\,\mathrm{d}S + \int_V \rho\mathbf{b}\,\mathrm{d}V$$

Generic transport equation for scalar quantities:

$$\frac{\mathrm{d}}{\mathrm{d}t}\int_V \rho\phi \,\mathrm{d}V + \int_S \rho\phi(\mathbf{v}-\mathbf{v}_\mathrm{b})\cdot\mathbf{n}\,\mathrm{d}S = \int_S \Gamma\nabla\phi\cdot\mathbf{n}\,\mathrm{d}S + \int_V \rho b_\phi\,\mathrm{d}V$$

Space-conservation law:

$$\frac{\mathrm{d}}{\mathrm{d}t}\int_V \mathrm{d}V - \int_S \mathbf{v}_\mathrm{b}\cdot\mathbf{n}\,\mathrm{d}S = 0$$

In these equations, ρ stands for fluid density, **v** is the fluid velocity vector and $\mathbf{v}_\mathrm{b}$ is the velocity of CV surface; **n** is the unit vector normal to CV surface whose area is S and volume V. **T** stands for the stress tensor (expressed in terms of velocity gradients and eddy viscosity), p is the pressure, **I** is the unit tensor, ϕ stands for the scalar variable (k or ε or ω), Γ is the diffusivity coefficient, **b** is the vector of body forces per unit mass and b_ϕ represents sources or sinks of ϕ. Since the CV can move arbitrarily, velocity relative to CV surface appears in the convective flux terms, and the time derivative expresses the temporal change along the CV-path.

To account for the free surface and allow for its arbitrary deformation (including fragmentation, trapping of air bubbles, etc.), an additional equation is solved for the volume fraction c of the gas phase, which can be treated either as an incompressible fluid or as a compressible ideal gas:

$$\frac{\mathrm{d}}{\mathrm{d}t}\int_V c \,\mathrm{d}V + \int_S c(\mathbf{v}-\mathbf{v}_\mathrm{b})\cdot\mathbf{n}\,\mathrm{d}S = 0$$

Liquid and gas are considered two immiscible components of a single effective fluid, whose properties are assumed to vary according to the volume fraction of each component as follows:

$$\rho = \rho_1 c + \rho_2(1-c)\ , \quad \mu = \mu_1 c + \mu_2(1-c)$$

It is beyond the scope of this paper to go into all the details of the numerical solution method, so only a brief description is given here; details can be found in [8].

All integrals are approximated by midpoint rule, i.e. the value of the function to be integrated is first evaluated at the center of the integration domain (CV face centers for surface integrals, CV center for volume integrals, time level for time integrals) and then multiplied by the integration range (face area, cell volume, or time step). These approximations are of second-order accuracy, irrespective of the shape of the integration region (arbitrary polygons for surface integrals, arbitrary polyhedra for volume integrals). Since variable values are computed at CV centers, interpolation has to be used to compute values at face centers and linear interpolation is predominantly used. However, first-order upwind interpolation is sometimes blended with linear interpolation for stability reasons. In order to compute diffusive fluxes, gradients are also needed at cell faces, while some source terms in equations for turbulence quantities require gradients at CV centers. These are also computed from linear shape functions.

In the equation for volume fraction of the gas phase, convective fluxes require special treatment. The aim is to achieve a sharp resolution of the interface between liquid and gas (one to two cells), which requires special interpolation of volume fraction. The method used here represents a blend of upwind, downwind, and central differencing, depending on the local Courant number, the profile of volume fraction, and the orientation of interface relative to cell face; for more details, see (Muzaferija et al 1999). The scheme is adjusted to guarantee that the volume fraction is always bounded between zero and one to avoid non-physical solutions.

The solution of the Navier-Stokes equations is found by using a segregated iterative method, in which the linearized momentum component equations are solved first using prevailing pressure and mass fluxes through cell faces (inner iterations), followed by solving the pressure-correction equation derived from the continuity equation (SIMPLE-algorithm; see (Ferziger et al 2003) for more details). Thereafter, equations for volume fraction and turbulence quantities are solved; the sequence is repeated (outer iterations) until all non-linear and coupled equations are satisfied within a prescribed tolerance, after which the process advances to the next time level.

3 PROPELLER DESCRIPTION

The two propellers used in this study are briefly introduced in this section. The cycloidal propeller is a 32R5 Voith Schneider Propeller (VSP) with a blade orbit diameter of 3.2m (Fig. 2).

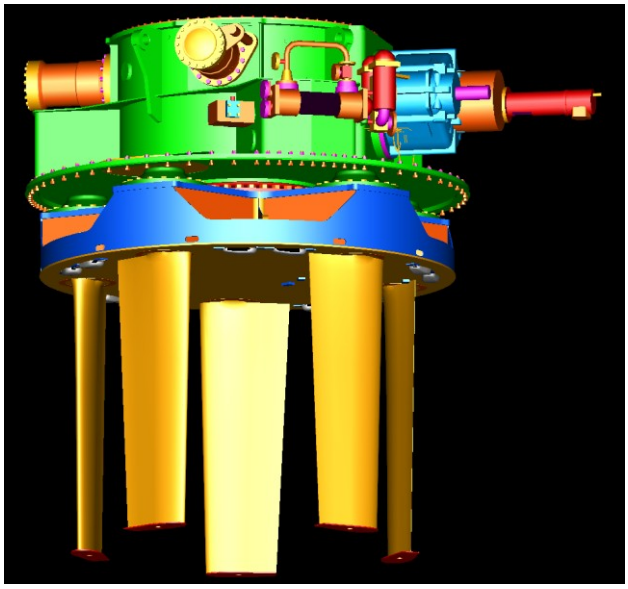

Fig. 2: Voith Schneider Propeller 32R5

The Voith Schneider Propeller, a controllable pitch propeller, generates thrust by means of profiled blades that protrude from the vessel bottom and rotate around a vertical axis. The blades are mounted in a rotor casing which is flush with the bottom of the vessel. A local oscillating motion of the individual propeller blades around their own axis is superimposed on the rotary motion of the blades around the common vertical axis. Generation of this oscillating motion is done via a kinematic mechanism. This working principle enables the propeller to adjust thrust continuously, both in amplitude and in direction. More details on the VSP principle can be found in Palm et al (2009) and Jürgens et al (2009).

The azimuth thruster used in the current study is a Voith Radial Propeller (VRP) with a propeller diameter of 4.2m (Fig. 3). This unit is equipped with a 98° bevel gear to implement the 8° inclined rotational axis. The fixed-pitch propeller is ducted with a high-efficiency nozzle for improved bollard pull performance.

4 EXPERIMENTAL SETUP

Scale model testing was carried out in Voith's circulation tank in Heidenheim. Fig. 4 shows the overall arrangement of that facility.

The tank has an open measuring section with a length of approx. 7m and a cross section of 2.2m x 1.1m. Flow speeds up to 4.5m/s can be achieved. Former comparative

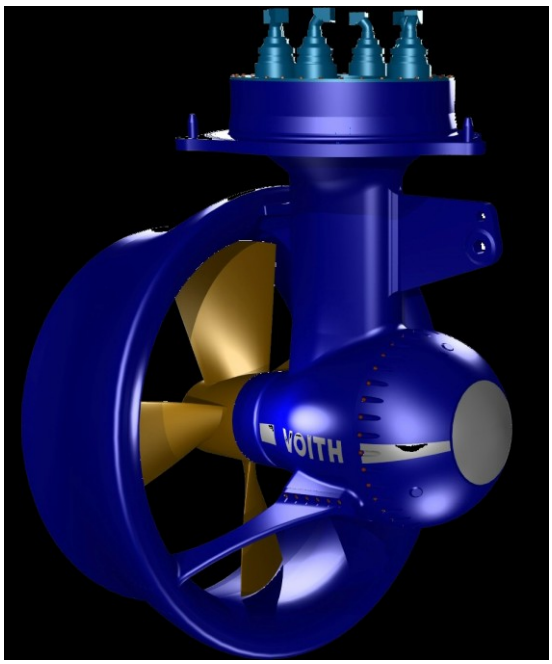

Fig. 3: Voith Radial Propeller 42-55

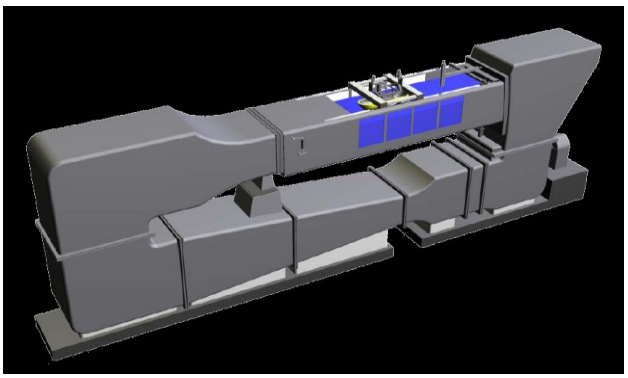

Fig. 4: Voith Circulation Tank

propeller measurements in large towing tank have shown that wall influences are negligible

The model of the Voith Schneider Propeller is shown in Fig. 5. The blade orbit diameter is 200mm and the blade length amounts to 165.6mm.

The propeller is installed below a generic ship hull. This body has a flat elliptical base area with a width of 645mm and a length of 2660mm. This arrangement was also considered in the CFD calculations conducted.

The overall torque, the total thrust and the number of revolutions are recorded during the measurements.

Fig. 5: Model Propeller VSP

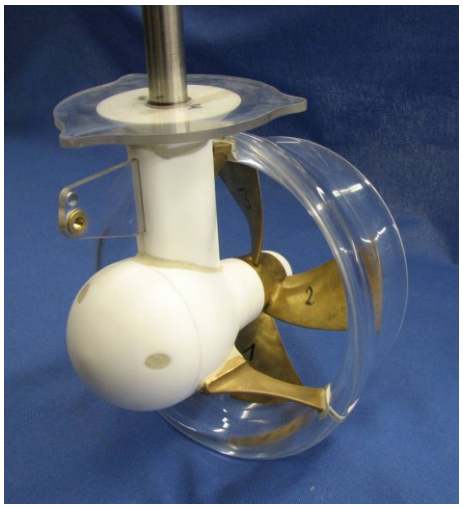

Fig. 6: Model Propeller VRP

The model for the Voith Radial Propeller has a propeller diameter of 210mm and is shown in Fig. 6. Thrust, torque and rotational speed are also measured.

Within the measurements and CFD calculations, the immersion of both propellers was varied by altering the distance h between the generic hull bottom and the water level. For better comparison, this value was non-dimensionalized with the total height d of the respective propulsor (see Fig. 7).

All measurements have been carried out for bollard pull conditions. Hence the inflow speed to the propeller was zero. The revolution speed was adjusted in a way that both propellers deliver approx. the same amount of thrust.

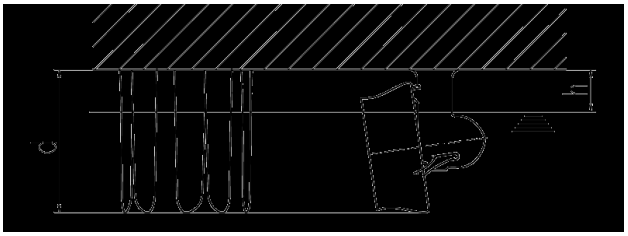

Fig. 7: Definition of Level of Immersion

Besides the geometrical and kinematic similarity, a couple of scaling numbers for dynamic similarity are important in this respect. The Reynolds number representing the ratio of inertia forces to viscous forces is difficult to keep constant in traditional model test facilities.

$$\mathrm{Re} = \frac{V_\infty c}{\nu}$$

Due to this limitation, the Reynolds number was about two orders of magnitude smaller than it would have been under full-scale conditions. Nevertheless, it is believed that this has no significant impact on the relative comparison between the two propeller types.

Given that two phases (air and water) are involved, surface tension effects may influence the investigation. The Weber number as the relevant scaling number is defined as

$$We = nD\sqrt{\frac{\rho D}{S}}$$

with n being the speed of revolution, D the propeller diameter and S the surface tension. In an extensive model test program (Shiba 1953), it was shown that the influence of the Weber number on the ventilation becomes insignificant at Weber numbers above 180. With Weber numbers around 190 this limit was well exceeded.

To account for wave-making effects the depth Froude number becomes relevant:

$$Fr = \frac{\pi nD}{\sqrt{gh}}$$

with h being the immersion. Additionally, the ventilation number gets important in this respect. It has a similar definition as the cavitation number, with vapor pressure being substituted by ambient pressure. The definition then simplifies to:

$$\sigma_V = \frac{p_\infty + \rho g h - p_\infty}{\frac{1}{2}\rho V_\infty^2} = \frac{2\mathrm{gh}}{\mathrm{V}_\infty^2}$$

Ventilation number similarity is automatically fulfilled if, at a given advance coefficient, depth Froude number similarity is fulfilled.

5 EXPERIMENTAL RESULTS

Some impressions on the ventilation phenomena can be seen in the following figures. Fig. 8 and Fig. 9 show the Voith Schneider Propeller and the Voith Radial Propeller at h/d=0.1 resp. h/d=0.04.

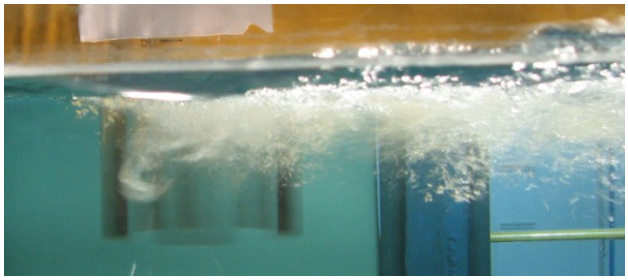

Fig. 8: Voith Schneider Propeller at h/d=0.1

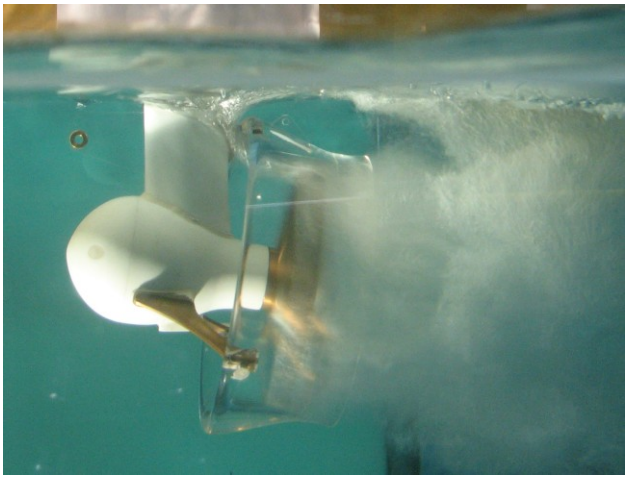

Fig. 9: Voith Radial Propeller at h/d=0.04

Although the propeller domain has not even pierced the free surface, the azimuth thruster has already started to draw air into the nozzle, leading to air entrapments over the whole propeller perimeter. Due to the different working principle of the VSP, the ventilation influence is limited to a certain distance from the free surface.

This qualitative difference is also reflected by the thrust measurements. Fig. 10 shows the thrust characteristics of both propeller types over the immersion ratio. The torque values indicate an almost identical behavior.

While the azimuth thruster experiences severe thrust reductions even at low immersion ratios, the losses for the cycloidal propeller are less pronounced. At a fairly low immersion ratio of 0.04 (Fig. 9), the VRP produces only 25% of its nominal thrust. The corresponding value for the VSP is roughly three times higher. The ratio of the thrust losses becomes larger as the immersion ratios increase. Generally, it can be concluded that the VSP thrust reduction runs closer to the linear degradation that is expected when ventilation effects are neglected.

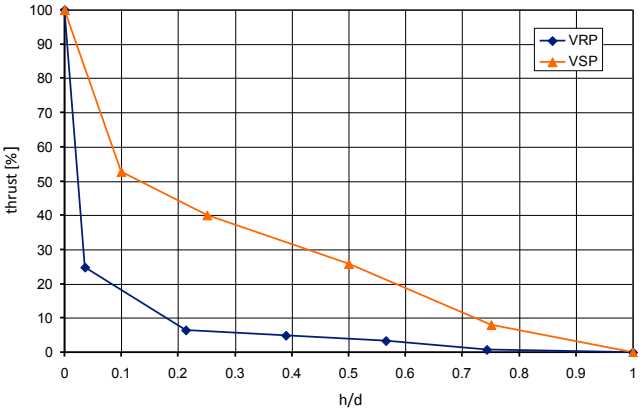

Fig. 10: Thrust Reduction over Immersion Ratio

6 NUMERICAL RESULTS

In addition to experimental studies, a large number of CFD calculations were carried out in order to gain more insight into ventilation phenomena.

For both propellers, many measured immersion ratios were also simulated. Fig. 11 shows the VSP results for three different immersion ratios.

The propeller is viewed from bottom showing the free surface deformation. The coloring on the blades indicates the pressure distribution.

The results show that only a small portion of the very left blade experiences some ventilation, while the remaining blades have no air contact in the immersed part.

The comparison between the experiments and the simulation is shown in Fig. 12. The thrust losses due to ventilation are well captured by the computational method. The torque reduction ranges are also similar.

The CFD results for the thruster type propeller are shown in Fig. 13. The high negative gradient of thrust reduction for small immersion ratios (Fig. 10) is well visualized. The air drawn directly affects the whole perimeter of the propeller. The suction side of the blade is already completely covered with air at h/d=0.21, which leads to thrust losses down to 5% of the nominal value.

The qualitative results of experiment and simulation are again similar. Only for small immersion ratios is the thrust reduction underestimated.

Experience shows that ventilation is also linked to thrust and torque fluctuations. The latter are believed to be responsible for fatigue failures in the power transmission train. Due to the transient simulations, force data per blade during one revolution is also available. Further comparisons were made with respect to blade force oscillations.

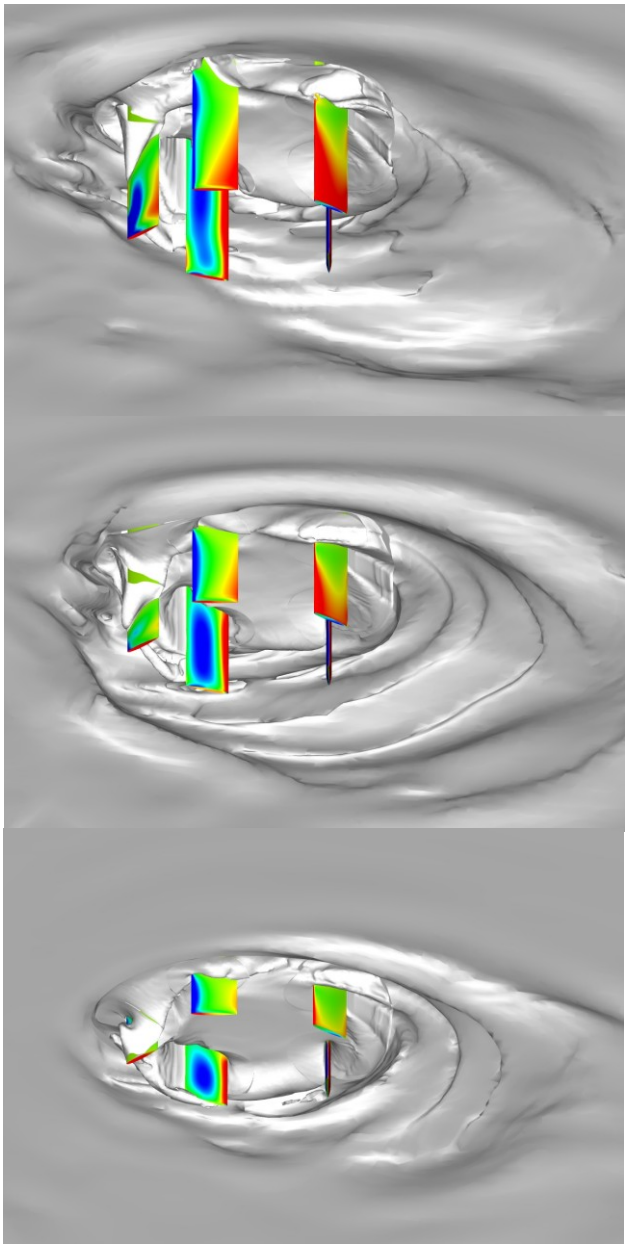

Fig. 11: VSP Results for h/d=0.25; 0.5 and 0.75

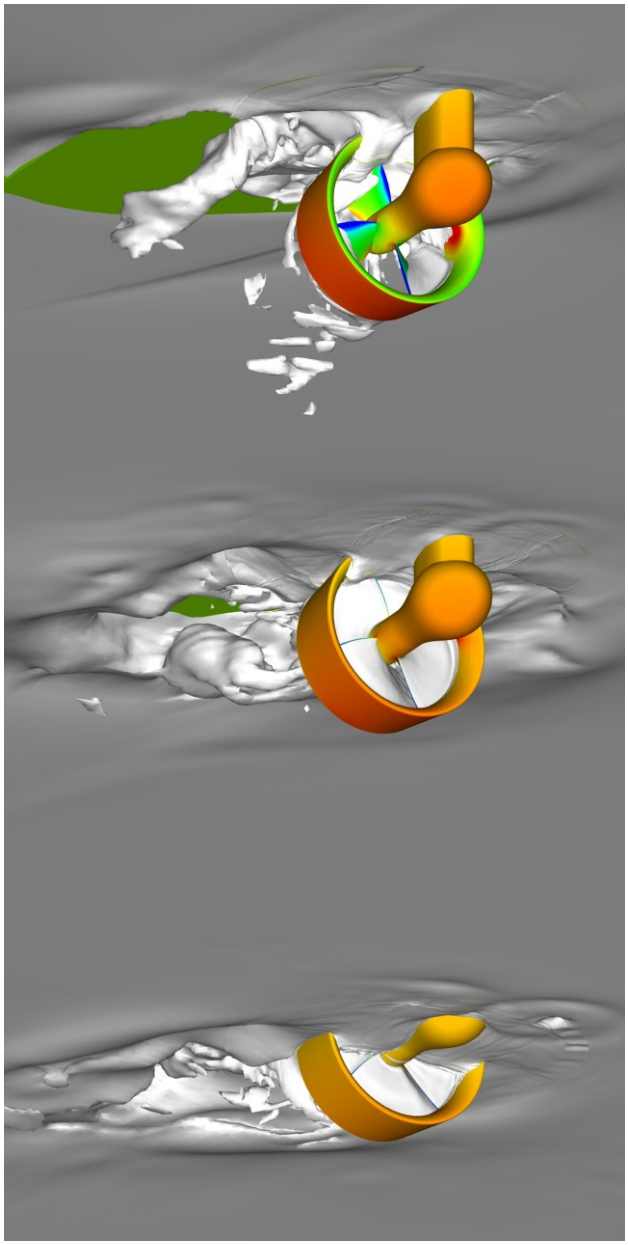

Fig. 13: VRP Results for h/d=0.04; 0.21 and 0.57

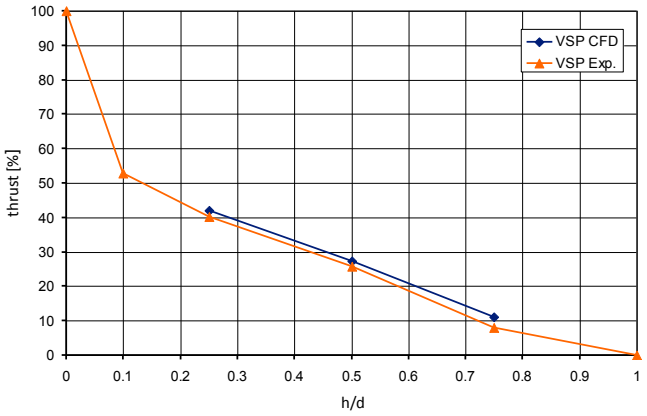

Fig. 12: VSP Thrust Reduction - Experiment and CFD

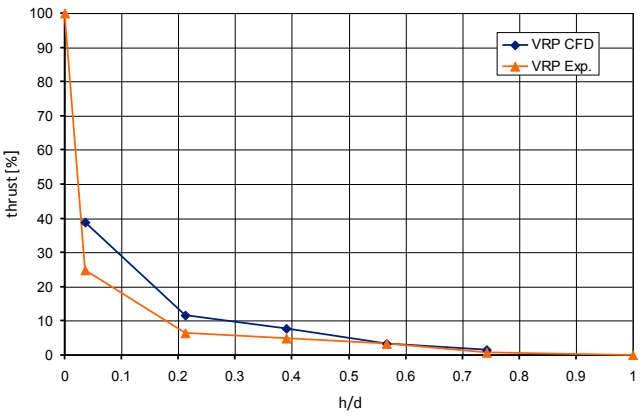

Fig. 14: VRP Thrust Reduction - Experiment and CFD

Fig. 15 compares the blade forces of the azimuth propeller for ventilating and non-ventilating conditions. The force is scaled with its maximum during one revolution.

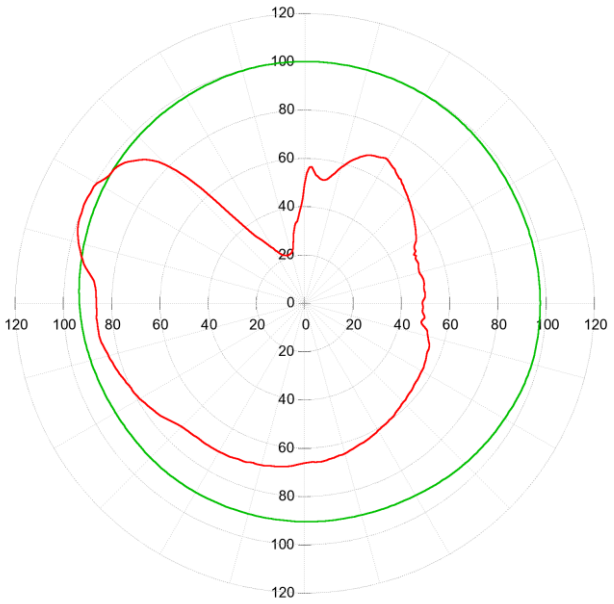

Fig. 15: VRP Blade Thrust Forces for Ventilating (Red) and Non-Ventilating (Green) Conditions h/d=0.04

It is evident that the blade thrust force is subject to large variations. For ventilating conditions, the blade thrust force drops down to 20% in the 12 o'clock position due to air entrapments. This force then slowly recovers to its maximum value after slightly more than ¾ of a revolution.

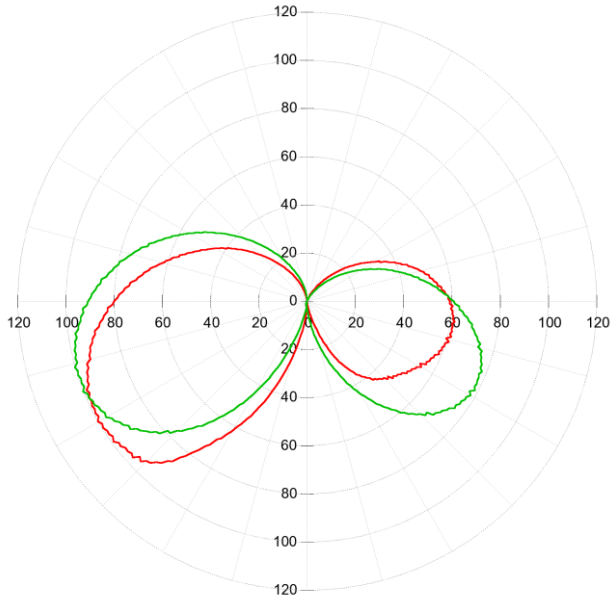

This can lead to load situations that might not have been considered in the design phase of the propeller.

Fig. 16: VSP Blade Thrust Forces for Ventilating (Red) and Non-Ventilating (Green) Conditions h/d=0.5

Due to its working principle, the corresponding curves for the VSP look very different. The two-stage thrust generation is visualized in Fig. 16. The large similarity of the blade thrust curves confirms the visual impression of smaller susceptibility to ventilation for cycloidal propellers. The progression of the curves for ventilating conditions has almost the same characteristic as the nominal curve.

7 CONCLUSION

The experiments as well as the numerical simulation revealed valuable insights into the ventilation characteristics of both propeller types examined. Due to its working principle, the cycloidal propeller is less prone to ventilation than the azimuth thruster.

Against the background of reported failures in bevel gears and other mechanical components which are believed to be related to ventilation incidents, the new data will be considered in the dimensioning process of the affected parts and will therefore contribute to higher reliability.

REFERENCES

Califano, A., Steen, S. (2009). 'Analysis of different propeller ventilation mechanisms by means of RANS simulations'. 1st Int. Symp. on Marine Propulsors, Trondheim, Norway.

Ferziger, J. H., Perić, M. (2003). Computational Methods for Fluid Dynamics. 3rd ed. Springer, Berlin.

Jürgens, D. & Heinke, H.-J. (2009). 'Voith Schneider Propeller - Investigations of the cavitation behavior'. 1st Int. Symp. on Marine Propulsors, Trondheim, Norway.

Koushan, K. (2004). 'Environmental and interaction effects on propulsion systems used in dynamic positioning'. PRADS2004, Lübeck, Germany.

Koushan, K. (2006a). 'Dynamics of ventilated propeller blade loadings on thrusters'. WMTC2006, London.

Koushan, K. (2006b). 'Dynamics of propeller blade and duct loadings on ventilated ducted thrusters operating at zero speed'. T-POD06, Brest.

Koushan, K. (2006c). 'Dynamics of ventilated propeller blade loading on thrusters due to forced sinusoidal heave motion'. 26th Symp. on Naval Hydrodynamics, Rome, Italy.

Koushan, K. (2007). 'Dynamics of propeller blade and duct loadings on ventilated ducted thrusters due to forced periodic heave motion'. Int. Conf. on Violent Flows, Fukuoka.

Muzaferija, S. & Perić, M. (1999). 'Computation of free surface flows using interface-tracking and interface-capturing methods'. Mahrenholtz & Markiewics (ed.) Nonlinear Water Wave Interaction, pp. 59-100, WIT Press, Southampton.

Palm, M., Jürgens, D. (2009). 'Voith Schneider Propeller - An efficient propulsion system for DP controlled vessels'. Dynamic Positioning Conference, Houston.

Shiba, H. (1953). 'Air drawing of marine propellers'. Report No.9, Transportation Technical Research Institute, Japan.